J|A|C|S
ARTICLES
Published on Web 09/29/2006

Insights into the Distribution of Water in a Self-Humidifying H_2/O_2 Proton-Exchange Membrane Fuel Cell Using ^1H NMR Microscopy

Kirk W. Feindel, Steven H. Bergens,* and Roderick E. Wasylishen*

Contribution from the Department of Chemistry, Gunning/Lemieux Chemistry Centre, University of Alberta, Edmonton, Alberta T6G 2G2, Canada

Received June 21, 2006; E-mail: roderick.wasylishen@ualberta.ca; steve.bergens@ualberta.ca

Abstract: Proton (^1H) NMR microscopy is used to investigate in-situ the distribution of water throughout a self-humidifying proton-exchange membrane fuel cell, PEMFC, operating at ambient temperature and pressure on dry $H_2(g)$ and $O_2(g)$. The results provide the first experimental images of the in-plane distribution of water within the PEM of a membrane electrode assembly in an operating fuel cell. The effect of gas flow configuration on the distribution of water in the PEM and cathode flow field is investigated, revealing that the counter-flow configurations yield a more uniform distribution of water throughout the PEM. The maximum power output from the PEMFC, while operating under conditions of constant external load, occurs when $H_2O(l)$ is first visible in the ^1H NMR image of the cathode flow field, and subsequently declines as this $H_2O(l)$ continues to accumulate. The ^1H NMR microscopy experiments are in qualitative agreement with predictions from several theoretical modeling studies (e.g., Pasaogullari, U.; Wang, C. Y. *J. Electrochem. Soc.* **2005**, *152*, A380−A390), suggesting that combined theoretical and experimental approaches will constitute a powerful tool for PEMFC design, diagnosis, and optimization.

1. Introduction

Proton-exchange membrane fuel cells (PEMFCs; see Figure 1) are an attractive alternative to traditional energy sources for applications including portable electronics, transportation, and large-scale stationary power generation.[1,2] An operating PEMFC for commercial use must be able to adapt to variations in power demand and operating conditions while maintaining near optimal performance. The power output, stability, and longevity of a PEMFC are affected by the quantity and distribution of water in the system[1−6] due, in part, to the properties of the PEMs used.[7] For example, when Nafion is used as the PEM, its proton conductivity improves as the water content increases.[8,9] Many factors influence the amount and distribution of water in an operating PEMFC including gas humidification and flow rates, power demands, and temperature. The quantity of water in the PEM is related to the electro-osmotic drag of water caused by proton conduction from the anode to cathode, and the transport of water from or into the feed gas streams. In addition, back-diffusion, that is, the transport of water through the PEM from the cathode to anode, results from the concentration gradient produced by the reduction of oxygen at the cathode.

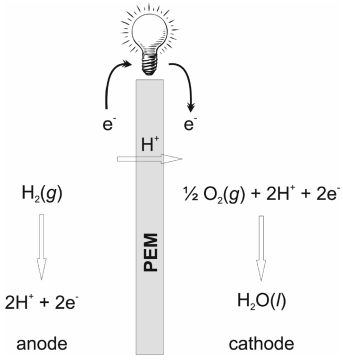

Figure 1. Representation of a PEMFC operating on $H_2(g)$ as fuel. $H_2(g)$ is oxidized over the anode catalyst, protons are transferred from the anode through the PEM to the cathode, and electrons are conducted through an external circuit. At the cathode catalyst, protons and electrons reduce $O_2(g)$ to produce $H_2O(l)$.

PEMFCs are an attractive alternative energy source due in part to their high theoretical energy efficiency of over 80% when operating on pure $H_2(g)$.[1] The demanding issue of delicate water balance for optimal performance, however, often requires the introduction of several parasitic components. For example, an air-fed PEMFC frequently requires a compressed cathode gas feed to increase the concentration of oxygen at the catalysts. To prevent dehydration of the PEM, both the anode and the cathode gas streams are often humidified externally at a

(1) Barbir, F. *PEM Fuel Cells: Theory and Practice*; Elsevier Academic Press: San Diego, CA, 2005.
(2) Hoogers, G., Ed. *Fuel Cell Technology Handbook*; CRC Press LLC: Boca Raton, FL, 2003.
(3) Larminie, J.; Dicks, A. *Fuel Cell Systems Explained*, 2nd ed.; John Wiley and Sons Ltd.: Chichester, 2003.
(4) St-Pierre, J.; Wilkinson, D. P.; Knights, S.; Bos, M. L. *J. New Mater. Electrochem. Syst.* **2000**, *3*, 99−106.
(5) Knights, S. D.; Colbow, K. M.; St-Pierre, J.; Wilkinson, D. P. *J. Power Sources* **2004**, *127*, 127−134.
(6) Atkins, J. R.; Savett, S. C.; Creager, S. E. *J. Power Sources* **2004**, *128*, 201−207.
(7) Hickner, M. A.; Pivovar, B. S. *Fuel Cells* **2005**, *5*, 213−229.
(8) Zawodzinski, T. A., Jr.; Derouin, C.; Radzinski, S.; Sherman, R. J.; Smith, V. T.; Springer, T. E.; Gottesfeld, S. *J. Electrochem. Soc.* **1993**, *140*, 1041−1047.
(9) Slade, R. C. T.; Barker, J.; Strange, J. H. *Solid State Ionics* **1989**, *35*, 11−15.

10.1021/ja064389n CCC: $33.50

temperature above the operating temperature of the PEMFC.[1−3] Ideally, a PEMFC would operate with stoichiometric flow rates of nonhumidified gases. Numerous experimental studies investigating the global performance of self-humidifying PEMFCs exist.[10−22] Büchi and Srinivasan reported[11] that the power output from a PEMFC operating with nonhumidified gases in both co- and counter-flow gas configurations was lower than that observed with external humidification. At low temperatures (<60 °C), self-humidification of the PEMFC was found sufficient for distributing water throughout the PEM without strict restrictions on gas flow rates or design. Learning to effectively manipulate parameters to maintain optimal cell performance is a critical juncture for commercialization of PEMFCs. The influence of each variable affecting an operating PEMFC must be understood, and in-situ diagnosis is required to achieve this goal.

Traditional fuel cell diagnostic methods provide crucial information regarding global performance characteristics (e.g., cell potential and resistance, Tafel slope,[23] concentration polarization, etc.) through numerical fitting of experimental polarization curves, and using techniques such as current interrupt and AC impedance spectroscopy.[1] These techniques do not, however, provide information regarding local water content or distribution. An important method by which insight into the amount and distribution of water in operating PEMFCs is obtained is through theoretical modeling. Many theoretical models to describe the thermochemical operation of PEMFCs have been developed to reproduce and predict experimental outcomes in an effort to engineer more efficient and reliable PEMFCs. An introduction to PEMFC modeling and representative examples can be found in a text by Barbir[1] and a more thorough summary in recent reviews.[24,25] Theoretical models are validated and improved with experimental data, and thus the capability of models is often impeded by a lack of detailed experimental information regarding what happens inside an operating PEMFC. To thoroughly understand, model, and optimize a fuel cell, the distribution of water must be known.

During the past decade, numerous experimental techniques were developed to measure or observe in-situ various phenomena within an operating PEMFC.[26−34] Since our review of the literature,[35] several neutron imaging studies have recently appeared describing the measurement of water distribution in operating PEMFCs.[36,37] Also, Schneider et al. have developed a method to simultaneously perform neutron imaging and locally resolved impedance spectroscopy.[38] Over the past 30 years, NMR spectroscopy investigations have,[39] and continue to,[40] improve the understanding of the morphology of PEMs and the state and behavior of water within them. We previously established that information regarding the distribution of water in the PEM surrounding the membrane electrode assembly, MEA, and in the gas flow fields of an operating PEMFC can be obtained using ^{1}H NMR microscopy.[27,35] ^{1}H NMR microscopy remains the only technique by which the distribution of water in the PEM can be isolated from water in the gas flow fields and gas diffusion layers, GDLs, in an operating PEMFC. Recently, Tsushima and co-workers used results from their NMR microscopy investigation measuring the cross-sectional water content in a 340 μm thick Aciplex-S containing MEA of an operating fuel cell[26] to parametrize a one-dimensional across-the-MEA water transport model.[41]

Here, we demonstrate that ^{1}H NMR microscopy can be utilized to study the in-plane variation of water contained in the PEM of an operating MEA. In particular, the dynamic interaction of cell power output, gas flow rates, and water content is investigated and visualized experimentally for the first time. Such information has long been sought, but continues to elude other methods currently used for in-situ PEMFC diagnosis. We examine the effect of co- versus counter-flow gas configurations on the in-plane distribution of water in the PEM and the flow channels of a PEMFC operating with dry H_2(g) and dry O_2(g). In addition, the effects of H_2O(l) accumulation in the cathode flow field on fuel cell power output are described, and our experimental observations are related to predictions from relevant theoretical models.

2. Experimental Section

The MEA was constructed via a hot-press decal-transfer method[42] with unsupported HiSpec 1000 Pt black and HiSpec 6000 Pt−Ru black for the cathode and anode catalyst (loadings ∼2−3 mg cm^{-2}), respectively. The geometric area of the catalyst decals was ∼0.5 cm^2. Nafion-117 was used as the PEM and Toray TGP-H-060 carbon paper as the gas diffusion layer, GDL, and current collector. Further details of the design and materials of the PEMFC used for this investigation are

(10) Sena, D. R.; Ticianelli, E. A.; Paganin, V. A.; Gonzalez, E. R. *J. Electroanal. Chem.* **1999**, *477*, 164−170.
(11) Büchi, F. N.; Srinivasan, S. *J. Electrochem. Soc.* **1997**, *144*, 2767−2772.
(12) Noponen, M.; Mennola, T.; Mikkola, M.; Hottinen, T.; Lund, P. *J. Power Sources* **2002**, *106*, 304−312.
(13) Yang, T. H.; Yoon, Y. G.; Kim, C. S.; Kwak, S. H.; Yoon, K. H. *J. Power Sources* **2002**, *106*, 328−332.
(14) Kwak, S. H.; Yang, T. H.; Kim, C. S.; Yoon, K. H. *J. Power Sources* **2003**, *118*, 200−204.
(15) Yang, B.; Fu, Y. Z.; Manthiram, A. *J. Power Sources* **2005**, *139*, 170−175.
(16) Qi, Z. G.; Kaufman, A. *J. Power Sources* **2002**, *109*, 469−476.
(17) Williams, M. V.; Kunz, H. R.; Fenton, J. M. *J. Power Sources* **2004**, *135*, 122−134.
(18) Benziger, J.; Chia, E.; Moxley, J. F.; Kevrekidis, I. G. *Chem. Eng. Sci.* **2005**, *60*, 1743−1759.
(19) Ge, S. H.; Li, X. G.; Hsing, I. M. *Electrochim. Acta* **2005**, *50*, 1909−1916.
(20) Zhu, X. B.; Zhang, H. M.; Liang, Y. M.; Zhang, Y.; Yi, B. L. *Electrochem. Solid-State Lett.* **2006**, *9*, A49−A52.
(21) Yu, H. M.; Ziegler, C. *J. Electrochem. Soc.* **2006**, *153*, A570−A575.
(22) Berg, P.; Promislow, K.; St Pierre, J.; Stumper, J.; Wetton, B. *J. Electrochem. Soc.* **2004**, *151*, A341−A353.
(23) Tafel, J. *Z. Phys. Chem.* **1905**, *50*, 641−712.
(24) Bıyıkoğlu, A. *Int. J. Hydrogen Energy* **2005**, *30*, 1181−1212.
(25) Cheddie, D.; Munroe, N. *J. Power Sources* **2005**, *147*, 72−84.
(26) Tsushima, S.; Teranishi, K.; Hirai, S. *Electrochem. Solid-State Lett.* **2004**, *7*, A269−A272.
(27) Feindel, K. W.; LaRocque, L. P. A.; Starke, D.; Bergens, S. H.; Wasylishen, R. E. *J. Am. Chem. Soc.* **2004**, *126*, 11436−11437.
(28) Stumper, J.; Haas, H.; Granados, A. *J. Electrochem. Soc.* **2005**, *152*, A837−A844.
(29) Patil, Y. P.; Seery, T. A. P.; Shaw, M. T.; Parnas, R. S. *Ind. Eng. Chem. Res.* **2005**, *44*, 6141−6147.
(30) Stoupin, S.; Chung, E.-H.; Chattopadhyay, S.; Segre, C. U.; Smotkin, E. S. *J. Phys. Chem. B* **2006**, *110*, 9932−9938.
(31) Bellows, R. J.; Lin, M. Y.; Arif, M.; Thompson, A. K.; Jacobson, D. *J. Electrochem. Soc.* **1999**, *146*, 1099−1103.
(32) Argyropoulos, P.; Scott, K.; Taama, W. M. *J. Appl. Electrochem.* **1999**, *29*, 661−669.
(33) Panchenko, A.; Dilger, H.; Möller, E.; Sixt, T.; Roduner, E. *J. Power Sources* **2004**, *127*, 325−330.
(34) Mosdale, R.; Gebel, G.; Pineri, M. *J. Membr. Sci.* **1996**, *118*, 269−277.
(35) Feindel, K. W.; Bergens, S. H.; Wasylishen, R. E. *ChemPhysChem* **2006**, *7*, 67−75.
(36) Zhang, J.; Kramer, D.; Shimoi, R.; Ono, Y.; Lehmann, E.; Wokaun, A.; Shinohara, K.; Scherer, G. G. *Electrochim. Acta* **2006**, *51*, 2715−2727.
(37) Hickner, M. A.; Siegel, N. P.; Chen, K. S.; McBrayer, D. N.; Hussey, D. S.; Jacobson, D. L.; Arif, M. *J. Electrochem. Soc.* **2006**, *153*, A902−A908.
(38) Schneider, I. A.; Kramer, D.; Wokaun, A.; Scherer, G. G. *Electrochem. Commun.* **2005**, *7*, 1393−1397.
(39) Mauritz, K. A.; Moore, R. B. *Chem. Rev.* **2004**, *104*, 4535−4585.
(40) Ye, G.; Janzen, N.; Goward, G. R. *Macromolecules* **2006**, *39*, 3283−3290.
(41) Teranishi, K.; Tsushima, S.; Hirai, S. *J. Electrochem. Soc.* **2006**, *153*, A664−A668.
(42) Cao, D. X.; Bergens, S. H. *Electrochim. Acta* **2003**, *48*, 4021−4031.

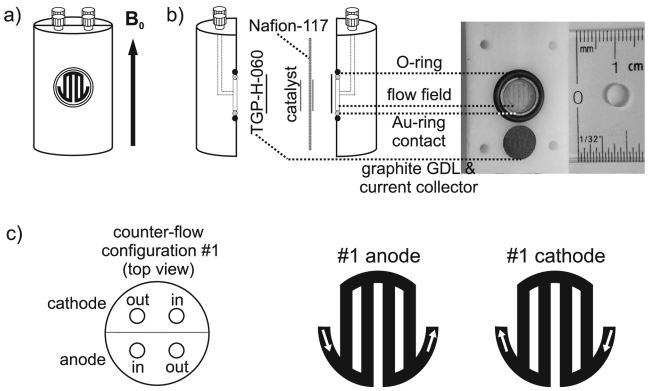

Figure 2. (a) Representation of the assembled PEMFC indicating the orientation and location of the flow fields, (b) assembly schematic and photograph indicating components and their location, and (c) counter-flow configuration #1 of gas inlets and outlets and direction of gas flow as viewed from anode to cathode.

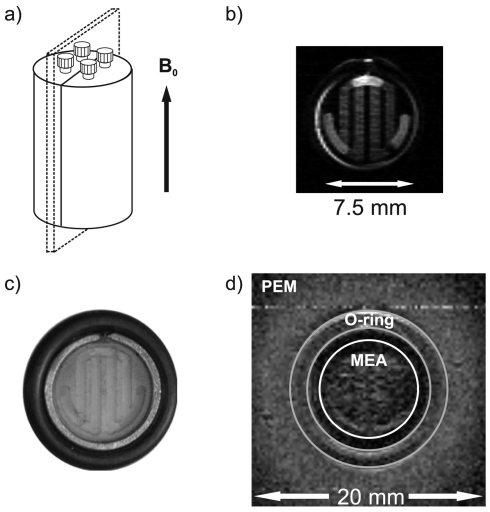

Figure 3. (a) Representation of the assembled PEMFC indicating the orientation of an NMR microscopy image slice, (b) ^{1}H NMR microscopy image from a 750 μm thick slice containing a flow field filled with water, (c) a photograph of the O-ring, Au-ring, and flow field, and (d) ^{1}H NMR microscopy image from a 500 μm thick slice containing the MEA with the location of respective components labeled.

described in detail elsewhere.[27,35] Prepurified H_2(g) (99.995%) and industrial grade O_2(g) (99.0%) obtained from Praxair were supplied at ambient pressure to the PEMFC from compressed gas cylinders via flow meters. The current drawn from the cell was controlled via a rheostat, and the current and voltage were monitored using Radio Shack 22-805 multimeters.

^{1}H NMR microscopy experiments were performed using a 7.05 T wide bore superconducting magnet, Bruker Avance 300 console, Micro-2.5 imaging accessory, and 30 mm birdcage resonator. The water-cooled gradient unit was maintained at 20 °C, and this was assumed to be the operating temperature of the PEMFC. A typical slice-selective spin−echo imaging sequence[43] was used to obtain images from a 30 mm × 30 mm field of view. The frequency encode direction was oriented parallel with the static applied magnetic field and the plane of the MEA (see Figure 2a). 128 frequency and phase encode steps were used, yielding an in-plane pixel size of 234 μm × 234 μm. In all experiments, the time between ^{1}H NMR signal excitation and acquisition of the first echo, T_E, was 3.2 ms, and in total eight echoes were summed after each excitation. The repeat time between successive ^{1}H NMR signal excitations, T_R, was 1.0 s, resulting in a total time of 128 s per image acquisition. In general, the PEM in an operating PEMFC is not saturated with water, and the ^{1}H spin−lattice relaxation time, T_1, of water is reduced significantly when in contact with paramagnetics such as the catalyst layers or O_2(g).[44,45] Therefore, $T_R = 1.0$ s is sufficiently long to prevent significant saturation of the ^{1}H NMR signal from water in the PEM. Difference images indicating the change in water content and distribution in the PEM were obtained by identifying the image with maximum water content in the PEM and subtracting the image representing minimum water content in the PEM. Experiments investigating the impact of gas inlet/outlet configuration were repeated a minimum of four times per configuration to confirm qualitative reproducibility of the observations.

3. Results and Discussion

3.1. The PEMFC. Representations of the PEMFC used for our investigations are shown in Figure 2a and b.[27,35] The fuel cell assembly consists of two half cylindrical blocks with gas inlets/outlets on the top. A gas flow field is machined into the face that presses against the graphite GDL/current collector. The planes of the MEA and the gas flow channels are oriented parallel with the direction of the applied magnetic field, $\mathbf{B}_0$ (see Figure 2a). The MEA is sandwiched between the cylinder halves and GDLs. Figure 2b shows a disassembled view of the PEMFC and a photograph of one-half of the cell that illustrates some of the components and their locations. We typically operate our PEMFC at 20 °C with dry H_2(g) and O_2(g) in a counter-flow arrangement with the gas inlets and outlets configured as indicated in Figure 2c. The direction of gas flow in the anode and cathode channels for this configuration, according to the perspective of ^{1}H NMR microscopy images shown herein (i.e., viewed from anode to cathode), is also illustrated in Figure 2c. The gas flow rates used herein are greater than stoichiometric requirements; however, in theory the water produced by the reduction of oxygen at the cathode is typically sufficient to fully hydrate the gases (see Supporting Information).

Figure 3a is a representation of the assembled PEMFC, indicating the orientation of a slice selected for ^{1}H NMR microscopy. An image obtained from a 750 μm thick slice containing a flow field filled with water is shown in Figure 3b. Note that, in the ^{1}H NMR microscopy images, a brighter region indicates a more intense NMR signal and thus a region with higher water content. Comparison of the photograph in Figure 3c with the images in Figure 3b and 3d shows the location of various components of the PEMFC in the ^{1}H NMR microscopy images. Typically, images of the operating PEMFC are acquired from a series of five parallel slices of 500 μm thickness oriented such that most of the MEA (Nafion-117, catalysts, and two GDLs) is contained within the central slice and the anode and cathode flow fields are contained in the neighboring slices. The image in Figure 3d was acquired from a 500 μm slice containing the MEA of the operating fuel cell. Note the presence of alternating dark and bright vertical stripes in the MEA region mimicking the location of the flow channels and ribs. Nafion-117 is known to swell from an initial thickness of ~177 to ~200 μm when in contact with H_2O(l),[46,47] consistent with our measurements.[35] The impact of MEA preparation procedures

(43) Callaghan, P. T. *Principles of Nuclear Magnetic Resonance Microscopy*; Oxford University Press: New York, 1991.
(44) Glasel, J. A. In *Water: A Comprehensive Treatise*; Franks, F., Ed.; Plenum Press: New York, 1972; Vol. 1.
(45) Hausser, R.; Noack, F. *Z. Naturforsch.* **1965**, *20A*, 1668−1675.
(46) Gebel, G.; Aldebert, P.; Pineri, M. *Polymer* **1993**, *34*, 333−339.
(47) Hinatsu, J. T.; Mizuhata, M.; Takenaka, H. *J. Electrochem. Soc.* **1994**, *141*, 1493−1498.

on the swelling properties of the PEM, however, has yet to be thoroughly investigated. In combination with the GDLs, each of 190 μm thickness, the upper limit for the total thickness of our MEA is ~580 μm. Although the image shown in Figure 3d was obtained from a 500 μm slice containing the MEA, in practice we have found that the ^{1}H NMR signal acquired results from water in the PEM only, herein referred to as H_2O(pem). Water contained in the catalyst layers or GDLs is difficult to observe due to the effect of the properties of the material on the ^{1}H NMR signal; rapid relaxation of the transverse magnetization (i.e., measurable NMR signal) results from several influences including the magnetic susceptibility differences, the electrical conductivity, and the paramagnetic nature of some materials.[35] Thus, ^{1}H NMR microscopy can provide a unique view of water within the PEM between the operating catalysts, separate from other regions of the PEMFC.

3.2. Distribution of Water in the PEM of the MEA. To initiate our investigations, a baseline condition of the PEMFC was first established. We found that a practical method to observe changes in water content and distribution in the operating PEMFC is to begin with no H_2O(l) in the flow fields and with the MEA at low water content. Using a ^{1}H NMR microscopy image of a low water content MEA as a reference allows separation of the effects of different water sources on distribution. For example, the growth and distribution of water from humidified gas streams can be observed if no current is drawn through the cell while the gases are flowing. The only source of water, then, would be from the humidified gas. In this study, we use dry gas streams to observe the water produced by the reduction of oxygen at the cathode (vide infra). The following indicates how gas flow rate, cell current, and ^{1}H NMR microscopy are used together to determine in-situ the effects of the amount of water on cell performance.

3.2.1. Removal of Water. Prior to operating the PEMFC, the anode flow field was filled with H_2O(l) to fully hydrate the PEM. After H_2O(l) was purged from the anode, the flow rates of the dry H_2(g) and O_2(g) were set to 5.0 and 2.5 mL min^{-1}, respectively. The power output was set to 24.8 mW cm^{-2} (21.0 mA, 0.590 V, electrode area ~0.5 cm^2) to allow the cell to establish a self-determined steady state of water in the MEA. Shown in Figure 4a are ^{1}H NMR microscopy images from 500 μm thick slices containing the MEA and the cathode flow field acquired from the PEMFC after operating for 35 min. During this period, a significant amount of H_2O(l) accumulated in the cathode flow field. The water originated from the fully hydrated PEM and from reduction of oxygen at the cathode. To remove this H_2O(l), we typically operate the PEMFC at a reduced current and increased O_2(g) flow rate. In general, flushing H_2O(l) from the cathode flow field is more difficult if the current drawn from the cell is not first reduced to decrease the amount of water produced. The current was reduced to 1.8 mA, and at $t = 0$ the O_2(g) flow rate was increased from 2.5 to 50 mL min^{-1}. The ^{1}H NMR microscopy images show that by $t = 5$ min (Figure 4b) most of the H_2O(l) was flushed from the cathode flow field, while the difference image indicates that water was not removed from the PEM. The H_2O(l) removed from the cathode flow field results in a slight increase in the cell voltage from 0.908 to 0.912 V at 1.8 mA. Once H_2O(l) is removed from the cathode flow field, the time required to remove H_2O(pem) is affected by the current drawn from the cell. Specifically, we found that higher currents typically dehydrate the PEM more rapidly. This effect is due to the increase in water transported through the PEM from the anode to the cathode via electro-osmotic drag.[48,49] The water produced at the cathode by reduction of oxygen cannot replenish the H_2O(pem) because of evaporation into the high flow of O_2(g). For example, after removing most of the H_2O(l) from the cathode flow field, at $t = 23$ min the external circuit load was changed to increase the cell power output to 29.5 mW cm^{-2} (20.8 mA, 0.709 V). After a brief improvement in performance due to complete removal of H_2O(l) from the cathode flow field, subsequent dehydration of the PEM resulted in a decrease in the cell power output. The images in Figure 4c, at $t = 26$ min, show that while there is still some H_2O(pem), the dark area in the central region of the difference image indicates that the amount of H_2O(pem)

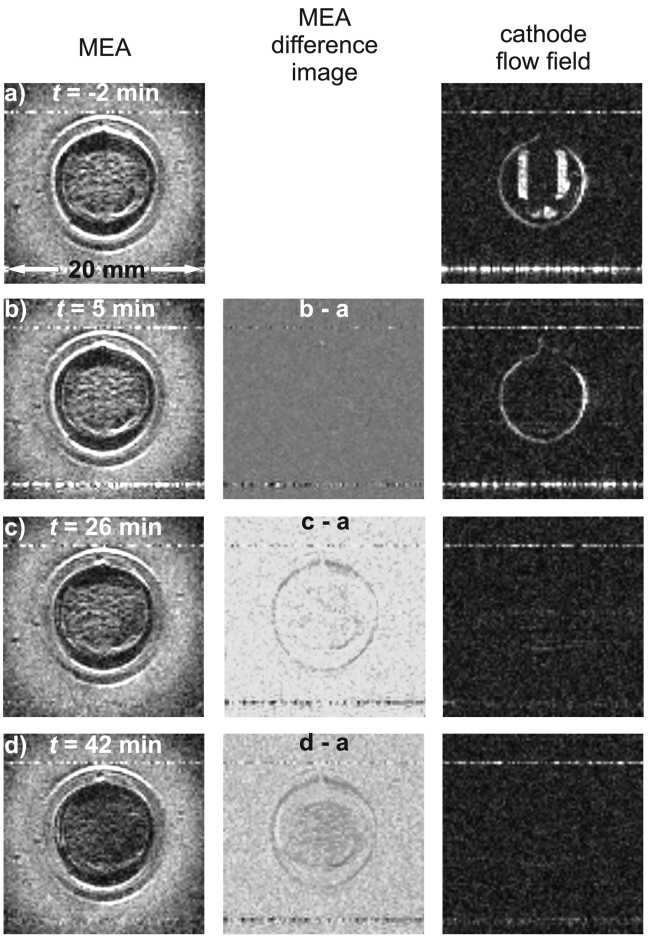

	Power / mW cm^{-2}	Current / mA	Potential / V
a)	3.3	1.8	0.908
b)	3.3	1.8	0.912
c)	31.8	21.6	0.736
d)	28.6	20.5	0.698

Figure 4. ^{1}H NMR microscopy images of the MEA (left), MEA difference images (center), and cathode flow field (right) obtained from the PEMFC operating on dry H_2(g) and O_2(g). $t = 0$ was when the O_2(g) flow rate was increased from 2.5 to 50 mL min^{-1}. See text for discussion.

(48) Ise, M.; Kreuer, K. D.; Maier, J. *Solid State Ionics* **1999**, *125*, 213−223.
(49) Kraemer, E. O.; Williams, J. W.; Alberty, R. A. In *A Treatise on Physical Chemistry*, 3rd ed.; Taylor, H. S., Glasstone, S., Eds.; D. Van Nostrand Co., Inc.: New York, 1951; Vol. 2.

remaining is slightly less than the amount at $t = -2$ min. At high O_2(g) flow rates, the PEMFC acts as a water pump, humidifying the gas stream with H_2O(pem) and water produced by the reduction of oxygen. Further operation over the following 16 min to $t = 42$ min (Figure 4d) dehydrates the PEM to the extent that the cell's performance is affected, causing a decline from 31.8 mW cm^{-2} (21.6 mA, 0.736 V) at $t = 26$ min to 28.6 mW cm^{-2} (20.5 mA, 0.698 V).

The use of NMR microscopy in combination with monitoring cell performance demonstrates that a high O_2(g) flow rate can quickly remove H_2O(l) from the cathode flow field and initially improves power output. Subsequent dehydration of the PEM and decrease in power output occurs when the MEA is no longer in contact with H_2O(l) in the flow field. As well, for this counter-flow configuration, the difference images indicate that the removal of H_2O(pem) appears uniform in distribution. The images in Figure 4b−d represent a snapshot of the H_2O(pem) in transition to a steady state. Prolonged operation of the PEMFC with a high O_2(g) flow rate ultimately dehydrates the PEM such that the performance cannot be recovered without decreasing the gas flow rate and humidifying the gas(es).

3.2.2. Recovery of Water and Self-Humidification. The ^{1}H NMR microscopy images shown in Figure 5 illustrate the recovery of H_2O(pem) by water generated at the cathode of the operating fuel cell and the accumulation of H_2O(l) in the cathode flow field after the O_2(g) flow rate is decreased. The images in Figure 5a were acquired 3 min prior to decreasing the O_2(g) rate from 50 to 2.5 mL min^{-1}, and the top image therefore represents a low water content PEM. Reducing the O_2(g) flow rate slows the evaporation of water from the cathode to enable hydration of the PEM. Beginning with the low initial water content PEM facilitates the observation of this process. Seven minutes after reducing the O_2(g) flow rate, the amount of H_2O(pem) has increased (Figure 5b). This recovery is evident in the MEA image and in the bright area in the central region of the MEA difference image. As H_2O(l) begins to accumulate in the cathode flow field, the cell power output peaks at 42.6 mW cm^{-2} (33.1 mA, 0.644 V). Figure 5c and d shows that the amount of H_2O(pem) continues to increase, but, with sustained H_2O(l) accumulation in the cathode flow field, the cell power output declines. The difference images indicate that the recovery of H_2O(pem) is uniform and that the accumulation of H_2O(l) occurs in the outlet half of the cathode flow field. This demonstrates that the PEMFC is effectively self-humidifying. These experiments illustrate that ^{1}H NMR microscopy is an effective in-situ diagnostic tool for optimizing fuel cell operating conditions.

Proton transport in Nafion may occur via a combination of mechanisms[50,51] including translational self-diffusion, Grotthuss-type transport,[52] Fickian diffusion, and electro-osmotic transport introduced by the electric field from anode to cathode.[48] Electro-osmotic proton conduction involves the co-transport of water, and, per proton, more molecules of water are transported with increasing PEM water content.[48] The water content, translational self-diffusion rate, and electro-osmotic drag coefficient in Nafion-117 are known to be highest when the PEM is in contact with H_2O(l).[8] An experimental study by Büchi and Srinivasan[11]

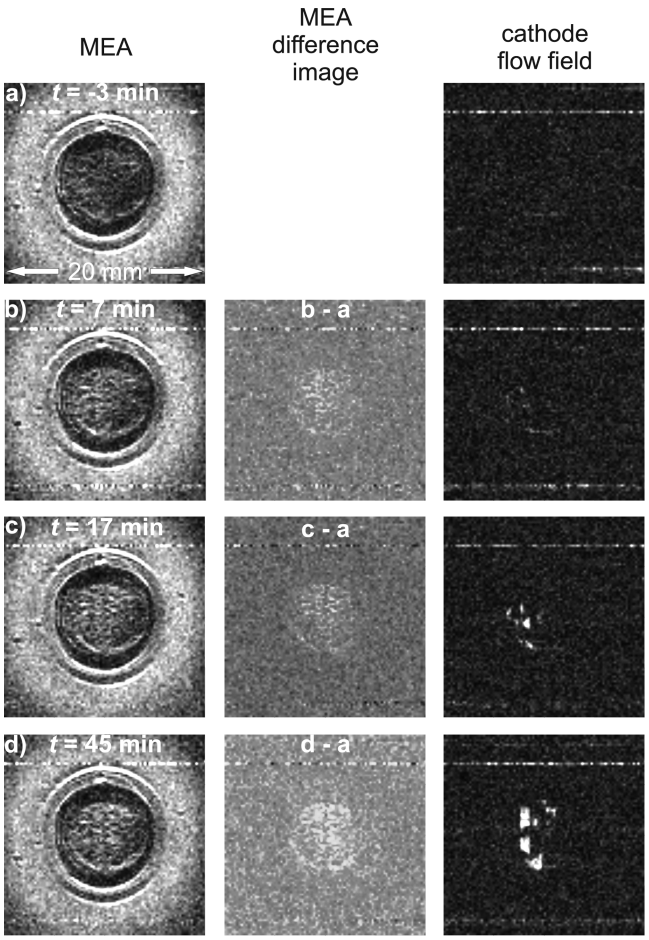

	Power / mW cm^{-2}	Current / mA	Potential / V
a)	37.7	31.1	0.606
b)	42.6	33.1	0.644
c)	41.9	32.8	0.638
d)	40.3	32.2	0.626

Figure 5. ^{1}H NMR microscopy images of the MEA (left), MEA difference images (center), and cathode flow field (right) obtained from the PEMFC operating on dry H_2(g) and O_2(g). $t = 0$ is when the O_2(g) flow rate was decreased from 50 to 2.5 mL min^{-1}. See text for discussion.

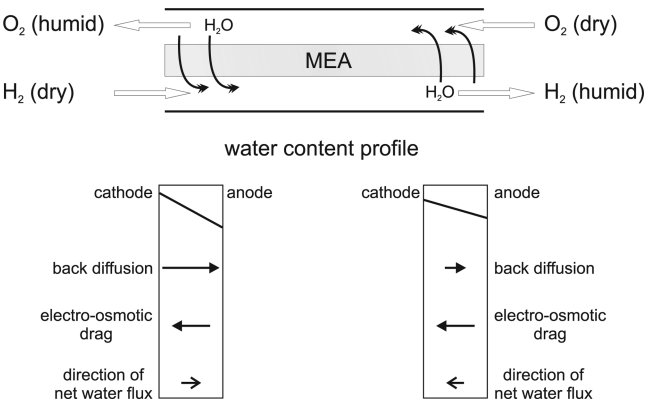

Figure 6. Schematic of the model postulated by Büchi and Srinivasan[11] for water flux across the MEA in a self-humidifying counter-flow PEMFC. See text for discussion.

(50) Kreuer, K. D.; Paddison, S. J.; Spohr, E.; Schuster, M. *Chem. Rev.* **2004**, *104*, 4637−4678.
(51) Paddison, S. J. *Annu. Rev. Mater. Res.* **2003**, *33*, 289−319.
(52) Agmon, N. *Chem. Phys. Lett.* **1995**, *244*, 456−462.

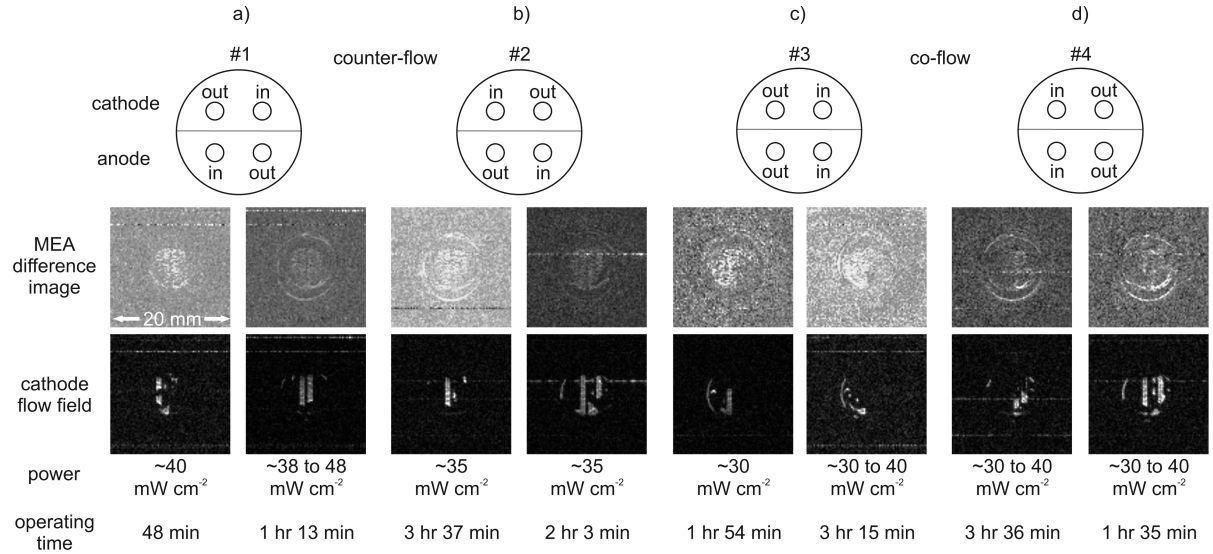

Figure 7. The four possible gas inlet/outlet configurations (top) and two representative examples of the resulting water distribution for each. The difference images (middle) show the distribution of water in the PEM relative to a low water content PEM. The cathode flow field images (bottom) show the location of $H_2O(l)$ accumulation.

of a fuel cell operating on dry anode and cathode gases in a counter-flow configuration led them to postulate a model for self-humidification of the gas streams (Figure 6). Several theoretical models for water transport in a PEMFC operating on dry reactant gases in a counter-flow arrangement predict similar behavior.[22,53−55] According to these studies, a water concentration gradient exists across the thickness of the MEA from the cathode to anode because water is only produced at the cathode. This phenomenon has also been previously observed with ^{1}H NMR microscopy.[26,41]

At the anode inlet/cathode outlet side of the cell, the water concentration gradient is largest because the anode gas enters dry and the cathode gas exits humidified by the water produced from the reduction of oxygen. Further, in our cell, $H_2O(l)$ produced at the cathode preferentially accumulates near the $O_2(g)$ outlet. In this region, the net flux of water across the PEM may be from cathode to anode; the concentration gradient may facilitate sufficient back-diffusion to surmount the water transported from anode to cathode via electro-osmotic drag. In addition, the local electro-osmotic drag coefficient may be reduced if catalytic sites are rendered inactive by the accumulation of $H_2O(l)$ in the cathode flow field. Now consider the anode outlet/cathode inlet side of the cell where the anode gas exits humidified and the cathode gas enters dry. In this region, the net flux of water is likely from the anode to the cathode. A water concentration gradient across the PEM from cathode to the anode remains; however, the magnitude of the gradient is smaller than at the cathode outlet. Therefore, the amount of water transported by back-diffusion from cathode to anode will be less than the amount of water transported from anode to cathode via electro-osmotic drag.

3.3. Influence of Gas Inlet/Outlet Configuration. We investigated the influence of the gas inlet and outlet configuration on the in-plane distribution of H_2O(pem), on the distribution of $H_2O(l)$ in cathode flow field, and on performance of the cell. Starting from an initial dry MEA condition as described in section 3.2.1, the cell was operated with all four of the possible gas inlet/outlet configurations shown in Figure 7 (top). The power output was adjusted to allow the amount of H_2O-(pem) to reach a constant level and to facilitate accumulation of $H_2O(l)$ in the cathode flow field. For each configuration, images are shown for two series of experiments.

Figure 7a and b shows images acquired from the cell operating in the two counter-flow gas configurations. As established by the difference images, the in-plane distribution of H_2O(pem) for both counter-flow configurations is uniform. As discussed above, in the counter-flow configurations the distribution of H_2O(pem) remains relatively uniform because the dry gases enter the cell directly across the MEA from the exiting humidified gases. This relatively uniform distribution of H_2O(pem) imparted by the counter-flow configurations will encourage more homogeneous proton conduction and catalyst activity across the MEA. Now looking at the cathode flow field, for both counter-flow configurations $H_2O(l)$ typically begins to accumulate in the outlet half of the cathode flow field. After operating for several hours at higher currents, or when the cell is operated with the PEM saturated with water immediately before operating the cell, $H_2O(l)$ blockages may also envelop central regions of the flow field.

Figure 7c and d shows images acquired from the cell operating in the two co-flow gas configurations. For both co-flow configurations, the distribution of H_2O(pem), indicated by the difference images, is not uniform; the area of the PEM near the gas inlets contains less water than the region of the PEM near the gas outlet, as predicted by several theoretical models (vide infra). We propose that the dry gases entering the flow fields in parallel on opposite sides of the MEA will draw water from the same region, and this will dehydrate the PEM at the inlets. We note that this nonuniform distribution of water from outlet to inlet will cause in-plane diffusion of water from regions of high to low water content. With the co-flow configurations, we find that longer operating times and/or increased cell currents are often required to facilitate $H_2O(l)$ accumulation in the cathode flow field. The resistance to proton transport through the PEM is known to increase as the amount of water in the

(53) Hsing, I. M.; Futerko, P. *Chem. Eng. Sci.* **2000**, *55*, 4209−4218.
(54) Janssen, G. J. M. *J. Electrochem. Soc.* **2001**, *148*, A1313−A1323.
(55) Ge, S. H.; Yi, B. L. *J. Power Sources* **2003**, *124*, 1−11.

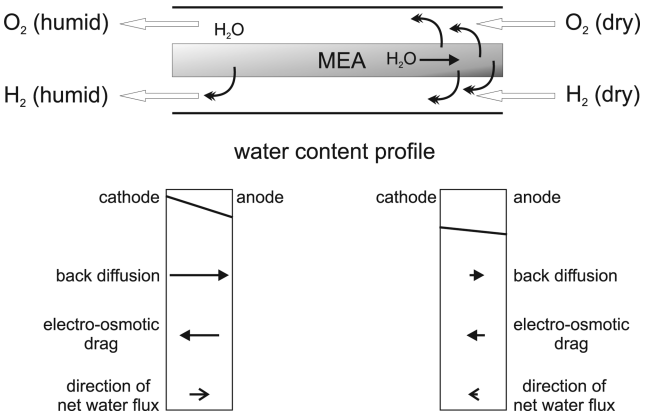

Figure 8. Schematic of a model for water flux across the MEA in a self-humidifying co-flow PEMFC. The darker shading indicates a region with low water content. See text for discussion.

PEM diminishes.[56,57] Therefore, regions of the PEM that contain less water will exhibit reduced proton transport, and, as a consequence, the catalysts over such a region of the PEM will operate less effectively. In addition, the resulting nonuniform distribution of potentials across the MEA will likely result in an in-plane proton current and an associated parasitic electron shunt current across the catalyst/electrode plane. We postulate that, in the absence of H_2O(l) in the cathode flow field, the distribution of H_2O(pem) represented by the NMR microscopy images indicates the relative activity of the operating catalysts in the MEA. Now considering the cathode flow field, in both co-flow configurations, H_2O(l) typically accumulates only in the outlet region. The second set of images for configuration #4, however, show that the distribution of H_2O(l) in the cathode flow field is more central. In effect, the lower half of the PEM toward the gas inlets is more hydrated in comparison to the same region in the first set of images for this configuration.

The performance of a PEMFC operating in a co-flow gas configuration with dry feed gases is often poor and unstable, and therefore most investigations of co-flow gas configurations typically incorporate humidification of one or both gas feeds. In general, co-flow models predict a low current density in the inlet region of low-humidity reactant gases due to the low water content of the membrane in this region.[22,55,58−60] Along the channel from gas inlet to outlet, the current densities and water content increase,[58−60] but current densities may decrease at the outlet if H_2O(l) is present.[55,61] These results suggest that net water flux across the membrane is toward the cathode near the inlets and toward the anode near the outlets.[58] A recent model investigating the effect of partial membrane drying predicted that along-the-channel nonuniformity of H_2O(pem) would generate a parasitic in-plane proton current.[62] Our observations provide the first direct experimental images of the nonuniform in-plane distribution of water in a PEMFC operating in co-flow gas configurations. To summarize various observations from

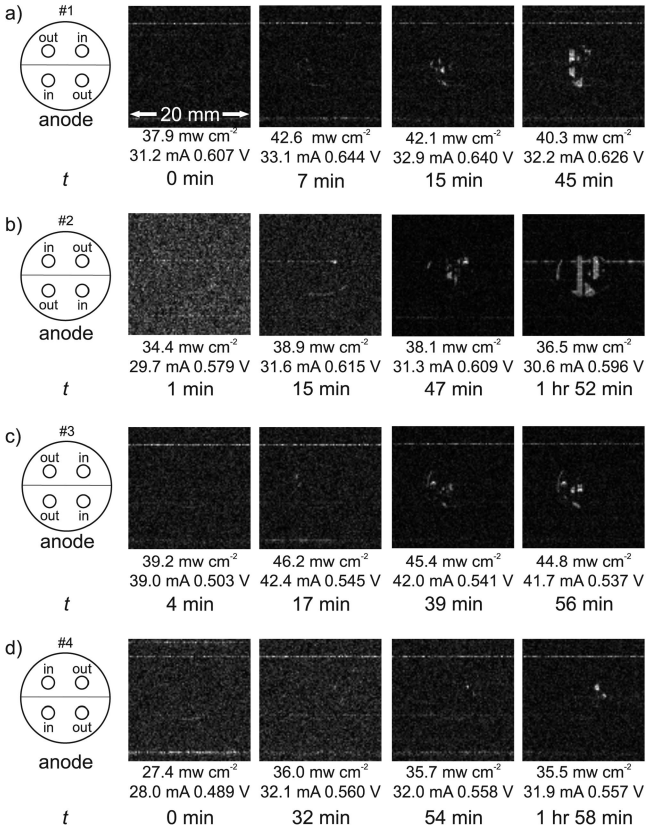

Figure 9. ^{1}H NMR microscopy images summarizing the effect of the onset of H_2O(l) accumulation in the cathode flow field and the subsequent impact of further water build-up. At $t = 0$, the O_2(g) flow rate was decreased to 2.5 mL/min. Note that the maximum performance observed for each configuration occurs at the onset of H_2O(l) accumulation (second image), followed by a slow decline in performance as water continues to build up in the cathode flow channels.

experiment and predictions from theoretical models, the schematic in Figure 8 illustrates our postulated flux of water in a dry or low-humidity co-flow PEMFC. Note, that in fuel cells with active areas of several 100 cm^2 with long gas flow channels and high flow rates, convective transport inside the channel dominates diffusion of water in the GDLs or PEM.[60]

Although H_2O(l) accumulates in the cathode flow field in both co- and counter-flow gas configurations creating a large concentration gradient from cathode to anode, we have not observed H_2O(l) in the anode flow field when using dry gas feeds. Therefore, in either co- or counter-flow configurations, achieving adequate back-diffusion to fully humidify the H_2(g) stream is unlikely. Thus, even at currents below that theoretically required to fully humidify both gas streams (see Supporting Information), cathode flooding may occur.

3.4. Effect of Accumulation of H_2O(l) in the Cathode Flow Field on Cell Performance. The task of maintaining the delicate balance of H_2O(pem) of an operating fuel cell such that ionic conductivity is maximized, while preventing the accumulation of H_2O(l) in the GDL and subsequently the cathode flow field, is difficult. We have often noted that the performance of our PEMFC is improved with a small amount of H_2O(l) in the cathode flow field. Thus, for each of the gas inlet and outlet configurations for our PEMFC, we investigated the relationship between the onset of H_2O(l) accumulation in the cathode flow field and the power output of the cell operated with a constant external circuit resistance.

(56) Siu, A.; Schmeisser, J.; Holdcroft, S. *J. Phys. Chem. B* **2006**, *110*, 6072−6080.
(57) Zawodzinski, T. A., Jr.; Springer, T. E.; Davey, J.; Jestel, R.; Lopez, C.; Valerio, J.; Gottesfeld, S. *J. Electrochem. Soc.* **1993**, *140*, 1981−1985.
(58) Pasaogullari, U.; Wang, C. Y. *J. Electrochem. Soc.* **2005**, *152*, A380−A390.
(59) Fuller, T. F.; Newman, J. *J. Electrochem. Soc.* **1993**, *140*, 1218−1225.
(60) Freunberger, S. A.; Santis, M.; Schneider, I. A.; Wokaun, A.; Büchi, F. N. *J. Electrochem. Soc.* **2006**, *153*, A396−A405.
(61) Dutta, S.; Shimpalee, S.; Van Zee, J. W. *J. Appl. Electrochem.* **2000**, *30*, 135−146.
(62) Kulikovsky, A. A. *Electrochim. Acta* **2004**, *49*, 5187−5196.

Figure 9 contains representative ^{1}H NMR microscopy images of the cathode flow field and PEMFC performance data for each of the four gas flow configurations. Prior to acquisition of each series of images, a high O_2(g) flow rate of 50 mL min^{-1} was used to remove H_2O(l) from the cathode flow field and to reduce the amount of H_2O(pem) (vide supra). The first image in each series was acquired at, or shortly after, $t = 0$ when the O_2(g) flow rate was decreased to 2.5 mL min^{-1}. Thus, the water that subsequently hydrates the PEM and accumulates in the cathode flow field is produced by the reduction of oxygen at the cathode. In all gas flow configurations (Figure 9a−d), the second NMR microscopy image in each series corresponds to the time at which H_2O(l) is first visible in the cathode flow field. For all configurations, the power output from the cell is highest at this time. The water content in Nafion-117 is known to be higher when in contact with H_2O(l) versus water vapor and results in a corresponding increase in ionic conductivity.[8] Before H_2O(l) is visible in the image of the cathode flow field, flooding of the catalysts and GDL must be occurring. As mentioned earlier, the NMR microscopy methods used herein do not reveal water at the catalyst surface or in the GDLs; however, a novel fluorescence microscopy technique for the ex-situ visualization of H_2O(l) transport in GDLs has recently been developed.[63] As H_2O(l) continues to build up in the cathode flow field (third and final images), the power output from the cell slowly declines. Only with more severe flooding of the cathode does a substantial decrease in cell performance occur.

A plethora of models have been developed to investigate the impact of gas flow configuration and/or gas humidification on the performance of fuel cells and along-the-channel water distribution (i.e., inlet to outlet),[58,59,61,64−69] including a number of studies investigating the impact of using both dry anode and dry cathode feed gases.[22,53−55,70] Variable water content in the PEM, and related properties, are often tied to the amount of water present in the gas along the flow channels. A recent study of water management in PEMFCs by Berg et al.[22] noted that capping the membrane water content in their model at a value below that expected for a PEM in contact with H_2O(l) may have contributed to some deviations of their model from experimental data. Few along-the-channel models, however, have incorporated the effects of the presence of H_2O(l) in the catalyst layer, GDL, or flow channels.[54,55,58,68] A two-phase model developed by Pasaogullari and Wang[58] predicted that for low-humidity cases the oxygen concentration decreased sharply at the onset of flooding in the GDL; however, at this point the cell also exhibited the highest current density for both of the under-humidified cases. Similarly, Sena et al. found that for a PEMFC operating between 298 and 310 K on dry H_2(g) and humidified O_2(g) or O_2/N_2 mixtures at atmospheric pressure, limiting effects due to oxygen diffusion to the catalyst were minimal. For Nafion-117, water transport through the membrane was found to become a limiting effect at high current densities.[10] Thus, at this juncture, in combination with our observations from experiment, we infer that for a low-humidity PEMFC operating at low current densities any detrimental effect on performance due to minimal accumulation of H_2O(l) at the catalyst layer or GDL is superseded by the improved ionic conductivity of the PEM when in contact with H_2O(l).

(63) Litster, S.; Sinton, D.; Djilali, N. *J. Power Sources* **2006**, *154*, 95−105.
(64) Bernardi, D. M.; Verbrugge, M. W. *J. Electrochem. Soc.* **1992**, *139*, 2477−2491.
(65) Nguyen, T. V.; White, R. E. *J. Electrochem. Soc.* **1993**, *140*, 2178−2186.
(66) Yi, J. S.; Nguyen, T. V. *J. Electrochem. Soc.* **1998**, *145*, 1149−1159.
(67) Futerko, P.; Hsing, I. M. *Electrochim. Acta* **2000**, *45*, 1741−1751.
(68) You, L. X.; Liu, H. T. *Int. J. Heat Mass Transfer* **2002**, *45*, 2277−2287.
(69) Cao, J.; Djilali, N. *J. Energy Resour. Technol.* **2005**, *127*, 26−36.
(70) Chan, S. H.; Goh, S. K.; Jiang, S. P. *Electrochim. Acta* **2003**, *48*, 1905−1919.

4. Conclusions

Using ^{1}H NMR microscopy, images of the in-plane distribution of water within the PEM of an MEA in an operating PEMFC were obtained for the first time. When the self-humidified PEMFC was operated with a high O_2(g) flow rate of 50 mL min^{-1}, the ^{1}H NMR microscopy images revealed that following removal of H_2O(l) from the cathode flow field, dehydration of the PEM ensued, resulting in a decline in the power output of the cell. Subsequent decrease of the O_2(g) flow rate to 2.5 mL min^{-1} resulted in an increase in content of water in the PEM, followed by accumulation of H_2O(l) in the cathode flow field. ^{1}H NMR microscopy was also employed to investigate the influence of co- versus counter-flow gas configurations on the in-plane distribution of water in PEM of the operating PEMFC. The co-flow configurations resulted in dehydration of the PEM at the inlets, while the counter-flow configurations effected a more uniform distribution of H_2O(pem). Also, at the onset of H_2O(l) accumulation in the cathode flow field, the power output of the cell peaks, while further build up of water results in a decline in power output. These observations are qualitatively in agreement with numerous theoretical fuel cell models.

This study demonstrates the unique ability of ^{1}H NMR microscopy to investigate in-situ the dynamic interplay of power output, gas flow rate, and water content and distribution in an operating PEMFC. Clearly, ^{1}H NMR microscopy will continue to reveal critical information regarding the distribution of water inside operating PEMFCs and is a powerful tool for diagnosing, understanding, and optimizing the effects of fuel cell materials, components, and designs.

Acknowledgment. Members of the solid-state NMR research group at the University of Alberta are thanked for helpful comments and discussions. Dr. Thomas Oerther at Bruker-Biospin GmbH is thanked for technical support. The PEMFC was designed in conjunction with, and machined by, Dieter Starke in the Department of Chemistry machine shop. We appreciate the assistance of the Department of Chemistry electronics shop. K.W.F. thanks the Natural Sciences and Engineering Research Council of Canada, NSERC, the Alberta Ingenuity Fund, and the University of Alberta for postgraduate scholarships. This research was funded by NSERC, the Canada Foundation for Innovation, Alberta Ingenuity, and the University of Alberta. R.E.W. thanks the Government of Canada for a Canada Research Chair in Physical Chemistry.

Supporting Information Available: Example calculation of the PEMFC current required for full humidification of the gas streams. This material is available free of charge via the Internet at http://pubs.acs.org.

JA064389N